Using EIS to study the electrochemical response of alloy AA5083 in solutions of NaCl

Einsatz der Elektrochemischen Impedanzspektroskopie (EIS) zur Untersuchung des elektrochemischen Verhaltens der Legierung AA5083 in NaCl-Lösungen

A. Aballe, M. Bethencourt, F. J. Botana*, M. Marcos and R. Osuna

The corrosion behavior of alloy AA5083 in aerated solutions of NaCl has been studied. Special attention has been paid to the analysis of the electrochemical response of this alloy using Electrochemical Impedance Spectroscopy (EIS). Analysis of the obtained data has enabled an evaluation of the contributions made by each of the corrosion processes active in the system: localized alkaline corrosion in the areas surrounding the intermetallic precipitates and growth of the layer of oxide on the matrix. It has been determined that the process of localized corrosion has the greatest verifiable intensity, but this process reduces with length of exposure time.

Das Korrosionsverhalten der Legierung AA5083 wurde in belüfteten NaCl-Lösungen untersucht. Besondere Aufmerksamkeit wurde der Analyse der elektrochemischen Reaktion dieser Legierung mittels Elektrochemischer Impedanzspektroskopie (EIS) gewidmet. Die Analyse der erhaltenen Daten ermöglichte eine Beurteilung der Anteile der einzelnen aktiven Korrosionsprozesse in dem System: lokale alkalische Korrosion in Bereichen, die die intermetallischen Ausscheidungen umgeben, und Wachstum der Oxidschicht auf der Matrix. Es wurde festgestellt, dass der Prozess der lokalen Korrosion die größte nachprüfbare Intensität aufweist, wobei dieser Prozess aber mit der Auslagerungsdauer abnimmt.

1 Introduction

In recent years, the use of Electrochemical Impedance Spectroscopy (EIS) has become extensive in the study of corrosion processes [1–9]. The fundamental reason for this increase is that, in principle, this technique provides information relating to the different processes that take place simultaneously in complex systems. Thus, using EIS, data can be obtained on the various sub-processes that make up the total corrosion process. It would be difficult to obtain such data by using other electrochemical techniques.

The capacity to provide information that discriminates between processes makes this technique especially attractive when analyzing processes associated with the different kinds of heterogeneities present in a system which, in most cases, could lead to phenomena of localized corrosion. Previously, EIS has been applied to the study of processes of pitting corrosion in various metallic alloys [10–14], to the analysis of the influence due to the presence of porosities in the layers formed in various ways on different metallic materials [15–20] and to the study of other types of process such as exfoliation and intergranular corrosion in aluminum alloys [21, 22].

In the present paper, EIS has been used to study the behavior of alloy AA5083 (Al-Mg) in aerated solutions of NaCl at 3.5%. Previous studies made of this alloy have revealed the presence of three types of intermetallic compound containing i) Al(Mn,Fe,Cr); ii) Al(Si,Mg); and iii) a ß(Al-Mg) phase [23, 24]. The presence and distribution of these compounds, particularly those of Al(Mn,Fe,Cr), condition the general behavior of alloy 5083 in the solution studied [23–27]. From the analysis using EIS, it is possible to differentiate the contributions to the total response of the system due i) to the reactions related to the presence of these intermetallic compounds; ii) to the existence of a layer of oxide on the matrix; and iii) to phenomena of transport across the metal-oxide interface. Monitoring over time has enabled the analysis of the evolution of each sub-process and its correlation with the results obtained by other techniques.

2 Experimental

Samples of alloy AA5083 of 30 × 25 × 4 mm were used; its nominal composition is given in Table 1. Prior to the tests,

* *F. J. Botana, A. Aballe, M. Bethencourt, R. Osuna*
Departamento de Ciencia de los Materiales e Ingeniería Metalúrgica y Química Inorgánica. Facultad de Ciencias del Mar. Universidad de Cádiz.
c/ República Saharaui s/n, Facultad de Ciencias del Mar, Puerto Real, E-11510 Cádiz (Spain)

M. Marcos
Departamento de Ingeniería Mecánica y Diseño Industrial. Escuela Superior de Ingeniería. Universidad de Cádiz.
c/ Sacramento, 82, E-11003 Cádiz (Spain)

 0947-5117/01/0303-0185$17.50+.50/0

Table 1. Nominal composition in % mass, of the alloy AA5083
Tabelle 1. Nennzusammensetzung der Legierung AA5083 in Masse-%

Mg	Mn	Si	Fe	Ti	Cu	Cr	Al
4.9	0.5	0.13	0.3	0.03	0.08	0.13	Rest

the samples were wet-polished with SiC paper of up to 500 grits, de-greased with ethanol and rinsed carefully in distilled water. A Parc Versastat potentiostat was used to record the diagrams of corrosion potential against time using an Ag/AgCl electrode as reference electrode.

The impedance spectra were obtained using a SI 1287 potentiostat coupled to a Solartron 1255 frequency response analyzer, both controlled by computer using the Corrware and Zplot programs of Scribner. In general, the amplitude of the AC signal applied was 5 mV. The equivalent circuits simulating the electrochemical response of the system were constructed making use of the FT-ENGINE routine of the Equivalent Circuit option of the ZView program of Scribner.

3 Results and discussion

In [28], a study of the behavior of alloy AA5083 in aerated solutions of NaCl at 3.5% is conducted by Scanning Electron Microscopy (SEM) and EDS. In this study, it is shown that two types of corrosion processes take place in parallel, under the conditions of exposure studied. The first is related to the deterioration suffered by the zones of the matrix surrounding one of the types of precipitate present in the alloy, Fig. 1. Fig. 1(a) shows the metallographic image corresponding to a sample of the alloy newly-polished to mirror quality; the two main types of precipitate present in the alloy are indicated. These precipitates have been identified as Al(Mn,Fe,Cr) and Al(Si,Mg) [23,24]. Fig. 1(b) is an image of the same zone of this sample after 72 hours of immersion in the solution of NaCl at 3.5%. On comparing the Al(Mn,Fe,Cr) precipitates, the existence of a localized corrosion process in the areas surrounding these precipitates can be observed, this causes a noticeable change. In contrast, the Al(Si,Mg) precipitates remain unaltered.

According to [29], the intermetallic compounds of Al(Mn, Fe,Cr) are more cathodic than the aluminum matrix. This converts these precipitates into permanent cathodes and the reduction of oxygen to OH^- ions is produced on these cathodes [30]. This in turn produces a local increase in the pH, giving rise to the dissolution of the oxide layer in the area surrounding the precipitate [31]. Once this layer has been dissolved, the local alkalinization causes an intense attack on the matrix. The evolution of this process over time can lead to the physical separation of the precipitate from the matrix, provoking the formation of hemispherical pits, which can be seen in Fig. 2. On the other hand, according to [32], the Al(Si,Mg) compounds present an activity similar to that of the matrix; for this reason, no kind of attack is observed on these precipitates nor on the matrix surrounding them.

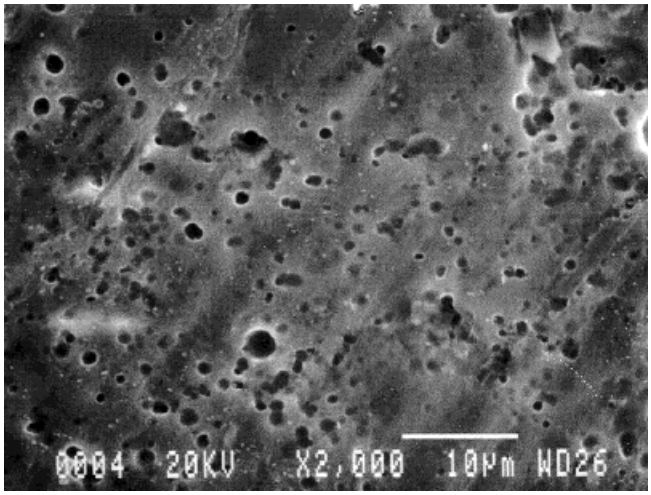

Fig. 2. SEM image of a sample descaled after 15 days of immersion in an aerated solution of NaCl at 3.5%. The hemispherical pits formed can be observed

Abb. 2. REM-Aufnahme einer entzunderten Probe nach 15 Tagen Tauchen in einer belüfteten 3,5% NaCl-Lösung. Die gebildeten rundlichen Löcher sind zu erkennen

In addition to the process of localized alkaline corrosion previously described, the matrix undergoes an oxidation process which gives rise to the formation of a layer of alumina, the thickness of which increases with exposure time, Fig. 3.

The transformations undergone by the alloy are also seen to be reflected in the values of the corrosion potential recorded as a function of the time of exposure. Fig. 4 is the E_{corr}-t diagram characteristic of a sample immersed for thirty days in an aerated solution of NaCl at 3.5%. In this figure, it can be observed

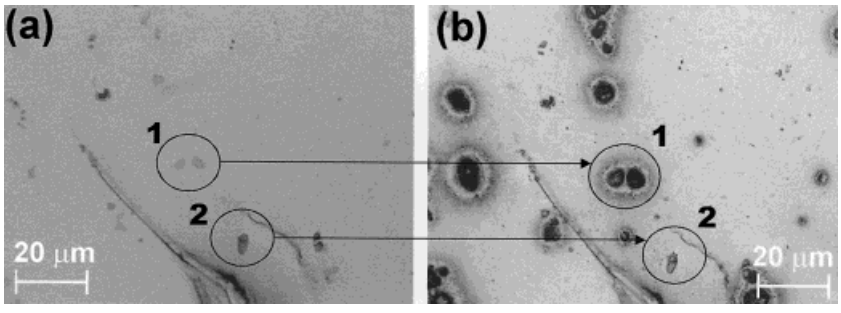

Fig. 1. Image taken with a metallographic microscope of a sample of alloy AA5083 before and after 72 hours of exposure in an aerated solution of NaCl at 3.5%. Point 1: Al(Mn,Fe,Cr) precipitate. Point 2: Al(Si,Mg) precipitate

Abb. 1. Mit einem metallographischen Mikroskop aufgenommenes Bild einer Probe der Legierung AA5083 vor und nach 72 Stunden Auslagerung in einer belüfteten 3,5% NaCl-Lösung. Punkt 1: Al(Mn,Fe,Cr) Ausscheidung. Punkt 2: Al(Si,Mg) Ausscheidung

how, at the very beginning of the exposure period, the potential of the sample takes a value of around − 0.850 V and then evolves to reach a value close to − 0.740 V after 5 hours. Then a slight decrease occurs until, after 20 hours of exposure, a virtually stable situation is reached in which the value of the potential is close to − 0.760 V. This open circuit potential value is maintained, with slight oscillations until the end of the 30 days period of exposure.

The E_{corr}-t records like that shown in Fig. 4 are characteristic of the behavior of aluminum and its alloys. In these, the initial value of the corrosion potential is determined in part by the ohmic drop caused by the natural film of oxide formed during the handling of the sample [33]. In addition, its value will be conditioned by the intensity of the cathodic process, which depends on the nature of the oxidizing agent and the cathodic areas existing in the alloy. If the film formed during the handling of the samples does not allow to reach the passive state, the metal will continue to oxidize until a new situation is reached that will depend on the characteristics of the alloy and of the corrosive medium [34]. The stage of growth of the oxide layer is reflected in the E_{corr}-t diagrams through the ennobling observed in the corrosion potential. Once an stationary situation is reached, the potential assumes an almost stable value, E_{st}. According to [35], the value of E_{st} depends on the velocity constants of the anodic and cathodic processes, on the relationship between the areas of the anodes and cathodes, on the thickness of the oxide film and on the concentration of the oxidizing agent.

In the magnification included in Fig. 4, it can be seen that, in the situation of stationary state, the potential does not really remain constant but rather continuous fluctuations are observed around a stable or horizontal trend. This would indicate that the situation reached by the system should not be classified as passivity but instead as stationary activity. According to [41], the displacements of the potential towards more active values must be related to the processes of activation that are verified in the anodic zones that encircle the cathodic precipitates. In agreement with the preceding comments, the local alkalinization of the medium causes the dissolution of the oxide leaving the matrix exposed, which in turn causes the jump of the potential towards more active values. The repassivation of these areas would cause the ennobling of the potential. At the same time, the decreases in potential could be explained as a consequence of falling away of the cathodic precipitates, Fig. 2. The superposition in time of all these events causes the appearance of noise observed in the records in Fig. 4.

One notable aspect is that, as can be observed in Fig. 4, during the entire period of exposure studied, the corrosion potential of the system is situated below the pitting nucleation potential, E_{pit}, the value of which is − 720 mV, as determined by linear polarization techniques, Fig. 5. This finding would explain the data obtained by SEM, according to which no crystallographic pits were observed during the entire period of exposure studied.

4 Measurements of electrochemical impedance

In accordance with the preceding comments, the surface of a sample of the alloy AA5083, before its exposure to the NaCl solution, may be represented by the scheme in Fig. 6. As shown in the diagram, the surface of the sample is covered by a fine layer of oxide generated during its handling. One of the characteristics of this film is the discontinuities presented in the zones occupied by the particles of the various intermetallic compounds that exist in the alloy. When the alloy is immersed in the NaCl solution, these zones are seen to be affected by a process of localized alkaline corrosion. In parallel, an increase in the thickness of the natural layer of oxide is produced. This growth implies the existence of a process of transport of Al^{3+} ions across this layer [36]. The overall elec-

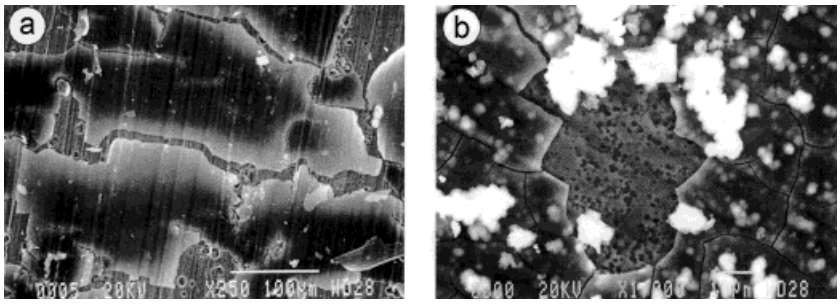

Fig. 3. Images of samples of alloy AA5083 showing the layers formed after (a) 15 days and (b) 30 days of immersion in an aerated solution of NaCl at 3.5%

Abb. 3. Bilder von Proben der Legierung AA5083, die die sich gebildeten Schichten zeigen: nach (a) 15 Tagen und (b) 30 Tagen Tauchen in eine belüftete 3,5% NaCl-Lösung

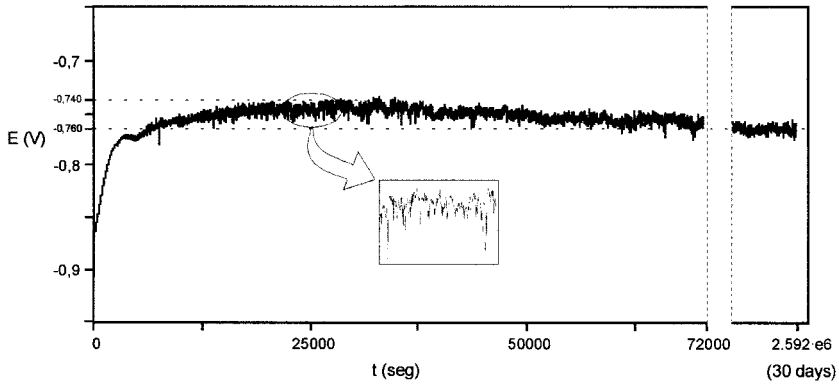

Fig. 4. Evolution of the open circuit potential of alloy AA5083 in a solution of NaCl at 3.5% during 30 days of immersion

Abb. 4. Entwicklung des Freien Korrosionspotentials der Legierung AA5083 in einer 3,5% NaCl-Lösung während 30 Tagen Tauchen

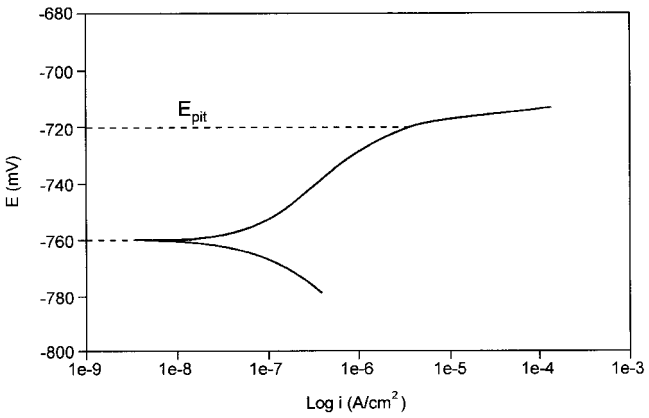

Fig. 5. Polarization curve of a sample of alloy AA5083 in a solution of NaCl at 3.5%, after 20 hours of immersion

Abb. 5. Polarisationskurve einer Probe der Legierung AA5083 in einer 3,5% NaCl-Lösung nach 20 Stunden Tauchen

trochemical response of the system will be the result of the superposition of these processes just described.

To reproduce the behavior of the system in terms of an equivalent electrical circuit, two alternatives have been considered. The first is based on one of the simplest models described in the bibliography for the simulation of the response of this type of system [37], Fig. 7. Using this model, the overall response of the system is obtained as a result of the superposition of the responses due to the film (R_C-C_C) and to the metal-oxide interface (R_T-C_{dl}). The elements (R_C-C_C) encompass all the information related both to the layer and to the possible defects there may be within it. On the other hand, all the processes of transport from the metal-oxide interface would remain included in the (R_T-C_{dl}) elemental loop.

The second of the models selected enables the evaluation separately of the contribution of each of the different kinds of processes found in the system. In particular, the attempt has been made to include a loop to evaluate the processes taking place in the zones occupied by the cathodic precipitates which, as has been stated previously, play a fundamental role in the behavior of alloy AA5083. In order to consider the response of these zones in the equivalent circuit, the model proposed in [37] has been modified, resulting in the circuit shown in Fig. 8. In this model, the loop R_C-C_C of the circuit in Fig. 7 has been divided into two loops R_{int}-C_{int} and R_{ca}-C_{ca}. The first of these is associated with the reactions that take place around the intermetallics. This type of modification has been proposed by various authors [38, 39] to take account of the processes found within the pores that exist in films and layers, or the presence of macroscopic defects in these layers [40]. In the model of Fig. 8, the response associated with the surface layer is represented by the loop R_{ca}-C_{ca}.

Each element in the circuits has been assigned on the basis of the time constants associated with each of the processes involved. The range of frequencies shown by each of these processes depends on these time constants. The results obtained previously indicate that the processes related to the presence of intermetallics take place almost immediately. For this reason, it is assumed that, when a spectrum of impedance is recorded, the response associated with the localized attack will be displayed in the high frequency range. The response of the surface layer will appear at slightly lower frequencies than that stemming from the localized alkaline corrosion process. Lastly, the slowest processes in the system, such as the transport of Al^{3+} ions across the oxide layer [36], will be displayed in the low frequency range.

The EIS data obtained in the study of the behavior of alloy AA5083 is given in Figs. 9, 10 and 11. In Fig. 9 are included the Nyquist and Bode diagrams corresponding to a sample of alloy AA5083 after two hours of immersion. As can be observed, the Nyquist diagram presents an initial well-defined arc, followed by a branch which could be assigned either to an unfinished second arc or to a diffusion tail. Included in the same figure are the simulated spectra after fitting the experimental data to the equivalent circuits of Figs. 7 and 8. It can be seen that in both cases there is a good fit between the simulated data and the experimental values. The values of each of the elements of the two circuits have been obtained from the simulated signals, Table 2. The mathematical equivalence between the two models studied is shown by proving, to a first approximation, the relationships:

$$R_{int} + R_{ca} = R_C \quad (1)$$

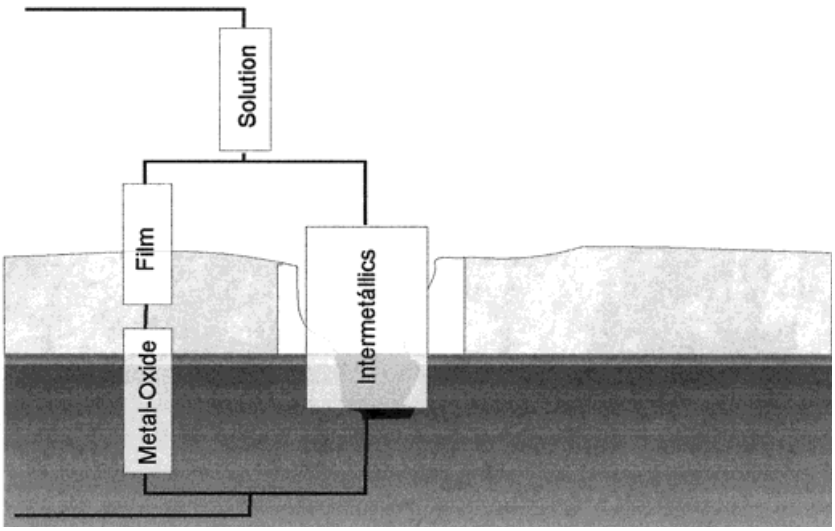

Fig. 6. Electrical diagram of the system including the contributions of each of the interfaces

Abb. 6. Elektrisches Diagramm des Systems einschließlich der Anteile der einzelnen Grenzflächen

Table 2. Values of the elements of the equivalent circuits of Figs. 7 and 8, fitted to the impedance spectra obtained in NaCl
Tabelle 2. Werte der Elemente der Analogieschaltkreise aus Abb. 7 und 8, angepasst an die in NaCl erhaltenen Impedanzspektren

time (hours)	R_e ($k\Omega \cdot cm^2$)	R_c ($k\Omega \cdot cm^2$)	C_c ($\mu F \cdot cm^{-2}$)	R_T ($k\Omega \cdot cm^2$)	C_{dl} ($\mu F \cdot cm^{-2}$)	R_{int} ($k\Omega \cdot cm^2$)	C_{int} ($\mu F \cdot cm^{-2}$)	R_{ca} ($k\Omega \cdot cm^2$)	C_{ca} ($\mu F \cdot cm^{-2}$)
2	$17 \cdot 10^{-3}$	39	12.07	62	111	$12 \cdot 10^{-3}$	6.46	38	5.18
6	$18 \cdot 10^{-3}$	26	11.54	47	189	0.62	9.50	24	1.39
11	$18 \cdot 10^{-3}$	36	10.92	49	226	0.59	8.92	34	1.39
19	$19 \cdot 10^{-3}$	52	10.62	68	244	0.47	8.73	50	1.45
24	$19 \cdot 10^{-3}$	98	238	64	10.42	0.38	8.62	62	1.47
36	$18 \cdot 10^{-3}$	206	141	66	10.24	0.34	8.27	62	1.57
42	$19 \cdot 10^{-3}$	81	10.04	180	158	0.59	8.34	76	1.28
49	$19 \cdot 10^{-3}$	108	9.80	185	166	0.58	8.15	93	1.27
54	$19 \cdot 10^{-3}$	120	9.69	267	148	0.66	8.05	112	1.24
75	$19 \cdot 10^{-3}$	141	9.60	172	173	0.62	7.85	132	1.40
105	$19 \cdot 10^{-3}$	221	9.41	148	206	1.04	8.25	210	0.90
135	$19 \cdot 10^{-3}$	364	150	788	8.67	1.30	7.50	695	0.69
195	$19 \cdot 10^{-3}$	626	8.13	990	79	0.83	7.27	598	0.74

$$C_{int} + C_{Ca} = C_C \quad (2)$$

In this way, it would be possible to analyze the system as a whole, making use of the model shown in Fig. 7, or else by analyzing the different contributions separately, by using the circuit in Fig. 8.

The evolution of the response of the system in the first 24 hours of exposure to the medium is given in the Bode diagrams included in Fig. 10. In the diagram |Z|-f, it can be observed that these initial hours of exposure are characterized by the existence of a fall in the value of |Z| which becomes steeper in the zone of lowest frequencies. This effect can be interpreted using the model in Fig. 8. Thus in Table 2, it can be confirmed that, in passing from 2 to 6 hours of exposure, the values of the capacities C_{int} and C_{ca} follow an inverse evolution. On the one hand, the value of C_{ca} undergoes a steep fall from 5.18 to 1.39 $\mu F/cm^2$. Accepting the expression:

$$C = \varepsilon\varepsilon_0 \, S.d^{-1} \quad (3)$$

for the capacity, this fall will be related to an increase in the thickness of the layer covering the matrix; this evolution would agree with that described on the basis of the record of corrosion potential against time. On the other hand, the value of C_{int} increases from 6.46 to 9.50 $\mu F/cm^2$. According to the model proposed, this variation will be related to the dissolution of the layer around the cathodic precipitates and the effective increase in the surface area of the matrix surrounding the precipitate. In Table 2 it can be seen that if the overall response of the layer is evaluated, by means of C_C, a compensation for the two effects is produced.

The effect of the time of exposure on the activity of the system should be reflected in the associated values of resistance. In Table 2, it can be seen that in all cases the value of R_{ca} is much greater than that of R_{int}, such that, in agreement with equation (2), the value of R_c is controlled by that of R_{ca}. Thus, when exposure time lengthens from 2 to 6 hours, a reduction is produced in the apparent resistance of the layer, R_C, as a consequence of the fall observed in the resistence R_{ca}. This fall observed in the value of R_{ca} will be related to the

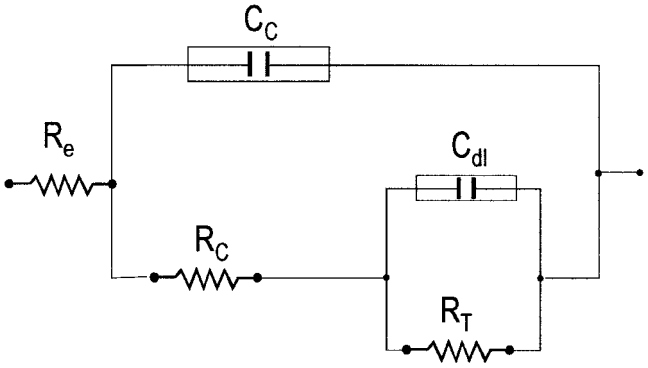

Fig. 7. Equivalent circuit of the system based on [42]
Abb. 7. Äquivalent-Schaltkreis des Systems basierend auf [42]

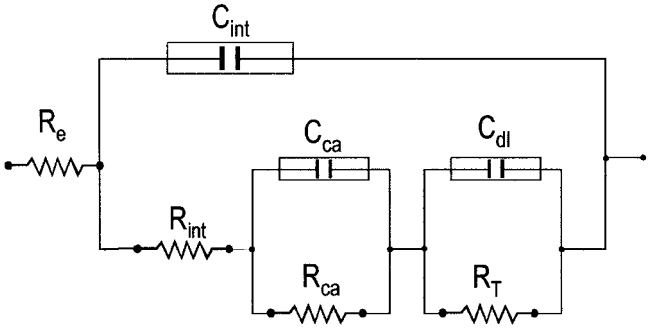

Fig. 8. Equivalent circuit proposed to reproduce the response of the system
Abb. 8. Vorgeschlagener Äquivalent-Schaltkreis, um das Verhalten des Systems wiederzugeben

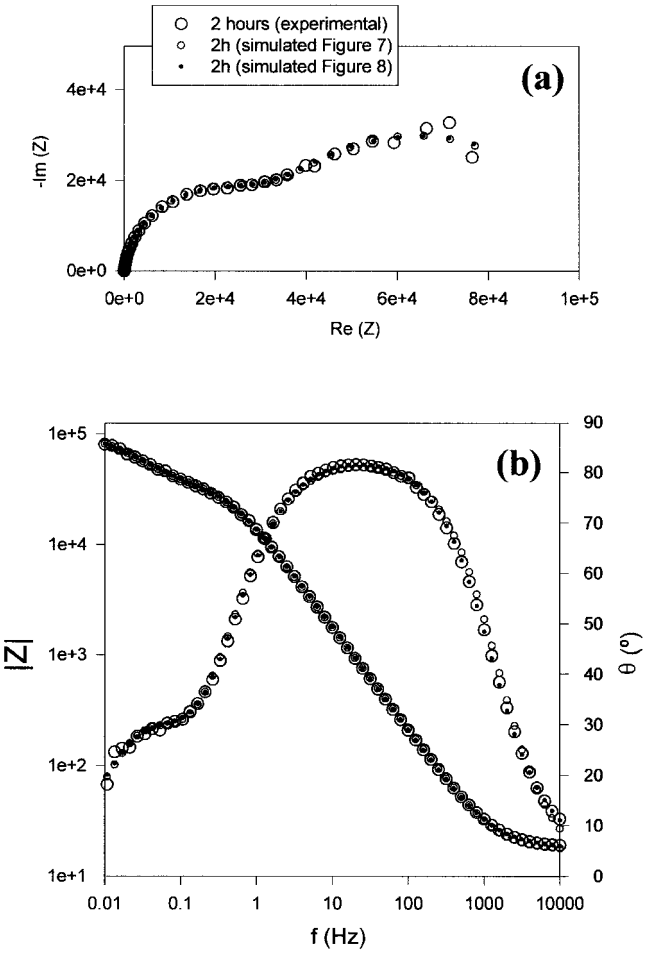

Fig. 9. Nyquist (a) and Bode (b) diagrams for a sample of alloy AA5083 after 3 hours of immersion in a solution of NaCl at 3.5%

Abb. 9. (a) Nyquist- und (b) Bode-Diagramme für eine Probe der Legierung AA5083 nach 3 Stunden Tauchen in einer 3,5% NaCl-Lösung

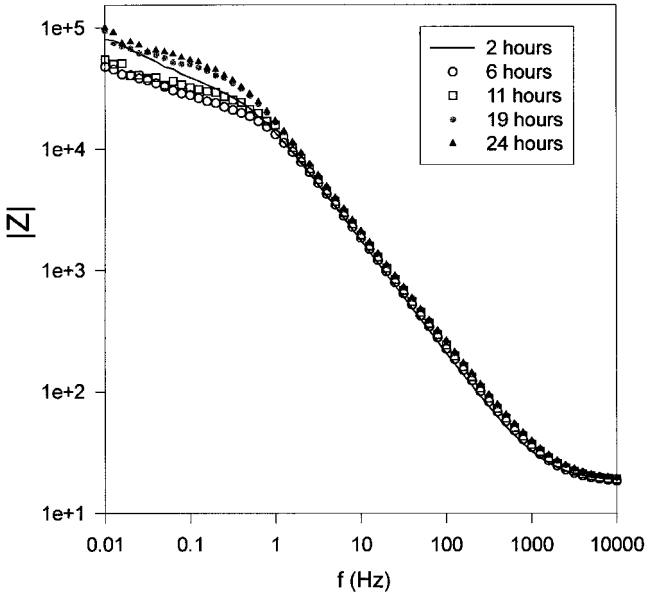

Fig. 10. Bode diagrams for the alloy AA5083 during the first 24 hours of exposure in a solution of NaCl at 3.5%

Abb. 10. Bode-Diagramme für die Legierung AA5083 während der ersten 24 Stunden der Auslagerung in einer 3,5% NaCl-Lösung

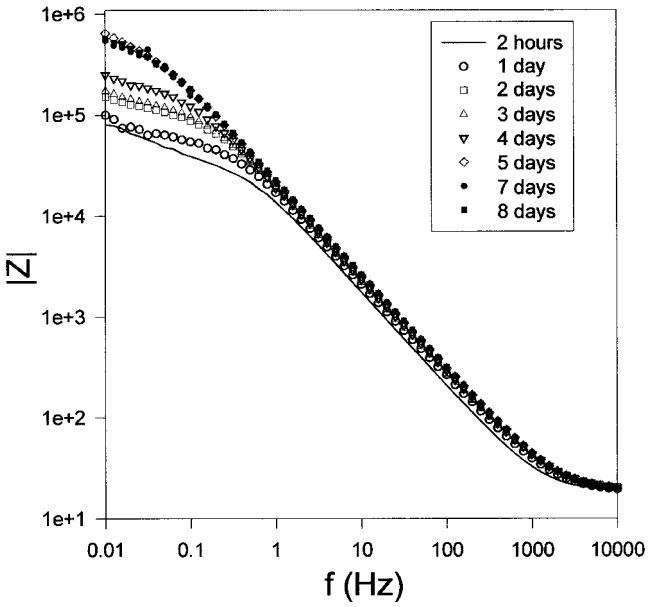

Fig. 11. Bode diagrams for the alloy AA5083 during the first 8 days of exposure in a solution of NaCl at 3.5%

Abb. 11. Bode-Diagramme für die Legierung AA5083 während der ersten 8 Tage der Auslagerung in einer 3,5% NaCl-Lösung

increase in activity necessary to produce the increase in the thickness of the layer. This activity generates an accumulation of charge on the external surface of the layer. According to [35], this accumulation of charge causes the appearance of image charges on the metallic surface, generating an electrical field which could be responsible for the reduction observed for R_T in this period of time, Table 2. Further, the increase in the value of R_{int} can be interpreted in terms of the reduction of the area of contact between the intermetallic particles and the matrix, similar to that which occurred with the capacity C_{int}.

Following from the preceding comments, the decrease in impedance observed in Fig. 10 can be related partly to the formation of the layer on the matrix, and partly to the increase in activity in the zones surrounding the cathodic precipitates.

The spectra obtained for the periods of exposure up to eight days are included in Fig. 11. In this, it can be observed how, with the passage of time, an increase occurs in the impedance of the system. Using the values included in Table 2, Figs. 12 to 14 have been constructed, in which the evolution over time of the different elements of the system is represented.

Thus, in Fig. 12 are represented the capacities C_C, C_{ca} and C_{int}. Firstly, it can be observed that the sharpest changes are those produced in the initial hours of exposure. Secondly, a notable difference exists between the values of C_C, C_{ca} and C_{int} which is maintained for the entire time interval studied. If these differences are interpreted in terms of thicknesses of film, this would mean that the thickness of the layer in the zones associated with the intermetallic compounds is maintained at considerably less thickness than on the rest of the surface. At the same time, when the model of Fig. 7 is used, a value for the apparent capacity of the layer, C_C , is obtained very close to that of C_{int} . In short, by using this model, information relating to the layer is lost.

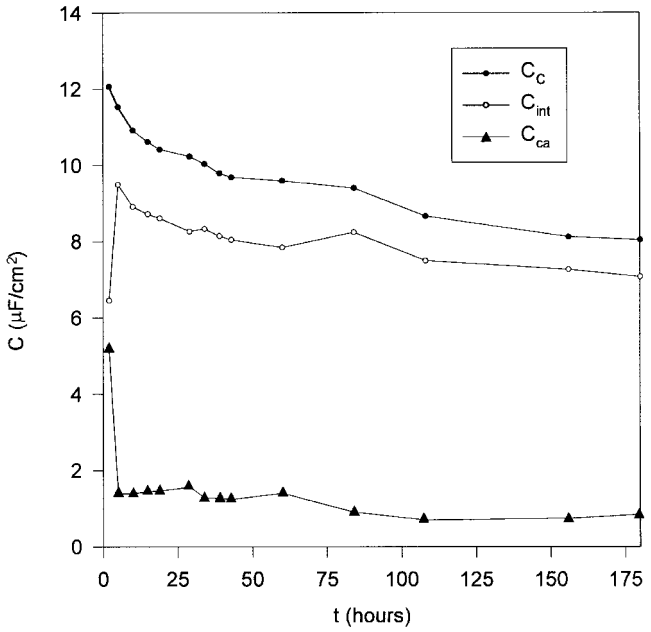

Fig, 12. Evolution over time of the capacities C_C, C_{ca} and C_{int}
Abb. 12. Entwicklung der Kapazitäten C_C, C_{ca} und C_{int} über die Zeit

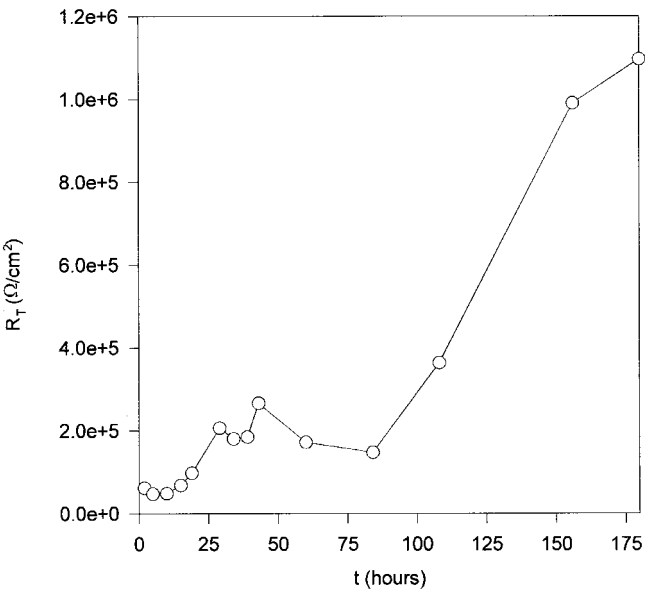

Fig. 14. Evolution over time of the resistance R_T
Abb. 14. Entwicklung des Widerstandes R_T über die Zeit

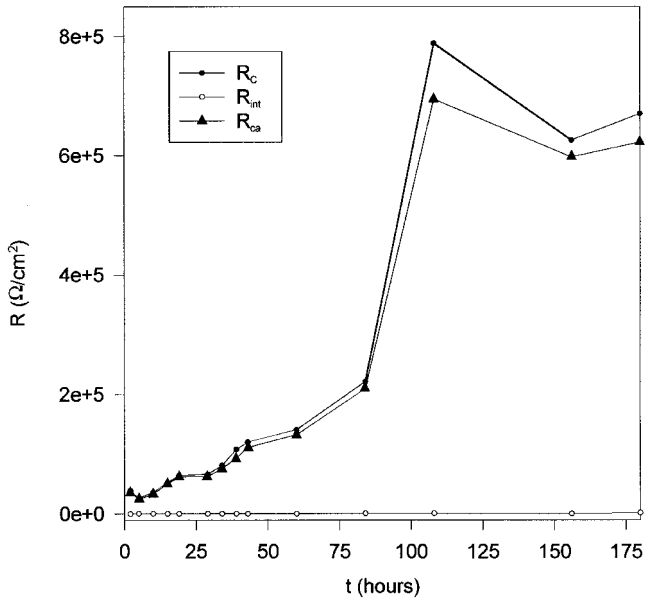

Fig. 13. Evolution over time of the resistances R_C, R_{int} and R_{ca}.
Abb. 13. Entwicklung der Widerstände R_C, R_{int} und R_{ca} über die Zeit

In Fig. 13 is represented the evolution over time of the resistances R_C, R_{int} and R_{ca}. In this figure, it can be seen that the value of R_C coincides, to a first approximation, with the value of R_{ca}. In addition, the values of both resistances follow a parallel evolution, with two clearly differentiated zones being defined. Thus, the first 60 hours of exposure are characterized by the values of both resistances increasing from 30 $k\Omega \cdot cm^2$ to 130 $k\Omega \cdot cm^2$. After 75 hours there is a sharp increase, with them reaching values of the order of 700 $k\Omega \cdot cm^2$. In parallel with this change in the resistances, a fall is observed in the value of C_{ca} from 1.40 $\mu F \cdot cm^{-2}$ to 0.90 $\mu F \cdot cm^{-2}$, Fig. 12. The changes observed in the values of R_{ca} and C_{ca} demonstrate that, for these times of exposure, a notable change must be produced in the properties of the layer. Evidently, these changes can be seen reflected in the values of R_T, Fig. 14.

Lastly, it can be observed in Fig. 13 that the value of R_{int} remains considerably lower than those corresponding to R_C and R_{ca}. In principle, this indicates that the activity associated with the zones corresponding to the precipitates is high in comparison with that found in other zones of the material. However, if the evolution of this parameter is analyzed in absolute terms, Table 2, it is observed how its value increases by two orders of magnitude with the passage of time. This would imply a decrease in the activity in these zones that could be related to the physical falling away of the intermetallic compounds as observed by SEM, Fig. 2.

5 Conclusions

When a sample of alloy AA5083 is immersed in an aerated solution of NaCl at 3.5%, basically two corrosion phenomena take place. Firstly, an increase is produced in the thickness of the natural oxide layer formed during the handling of the sample. Secondly, the zones encircling the Al(Mn,Fe,Cr) intermetallics are seen to be affected by a process of localized alkaline corrosion.

A study by EIS has been conducted of the electrochemical response of alloy AA5083 in an aerated solution of NaCl at 3.5%. This response has been simulated by using two different equivalent circuits. The first of these represents the overall electrochemical response of the layer and of the zones occupied by the intermetallic compounds, taken together. The second model allows the separate study of the individual contributions of the intermetallic compounds and of the film covering the matrix.

When the experimental data are fitted to the two model circuits proposed, it has been confirmed that the overall resistance of the layer is controlled by the resistance of the film covering the matrix. However, it has been confirmed that the apparent capacity of the layer is conditioned by the value of the capacity associated with the zones occupied by the intermetallics. This value is measurably lower than that of the capacity associated with the layer covering the rest of the sample. This would lead to the conclusion that, if the two-loop model is used to determine the thickness of the oxide film, a value much lower than that which really exists would be obtained. Therefore, if the aim is to measure correctly the thickness of the oxide film, the model with three loops should be used.

Furthermore, it has also been determined that the activity associated with the zones occupied by the cathodic precipitates is high, in comparison with that found in other zones of the material. This activity decreases in line with exposure time, falling by as much as two orders of magnitude after 8 days. In agreement with the observations made by SEM, this finding could be related to the physical separation of the intermetallic compounds from the surface of the alloy.

6 References

[1] *I. Epelboin, C. Gabrielli, M. Keddam, H. Takenouti:* ASTM STP-727 (1981)150.
[2] *F. Mansfeld:* Corrosion *37* (1981) 301.
[3] *W. J. Lorenz, F. Mansfeld:* Corros. Sci. *21* (1981) 647.
[4] *F. Mansfeld, M. W. Kendig, S. Tsai:* Corrosion *38* (1982) 552.
[5] *F. Mansfeld, M. W. Kendig:* Werkst. Korros. *36* (1985) 473.
[6] *M. W. Kendig, A. Allen, J. Jeanjaquet, F. Mansfeld:* Corrosion'85, Paper N° 74, NACE, Houston (USA), (1985).
[7] *M. Orazem, P. Agarwall, L. H. Garcia-Rubio:* Mater. Sci. Forum *192–194* (1995) 563.
[8] *F. Mansfeld:* Schlumberger TDI, Technical Report Number 26 (1993) I-16.
[9] "Electrochemical Impedance. Analysis and Interpretation". (Eds. J. R. Scully, D. C. Silverman, M. W. Kendig) ASTM STP 1188. American Society for Testing and Materials, Philadelphia (USA), (1993).
[10] *F. Mansfeld:* Electrochim. Acta *35* (1990) 1533.
[11] *F. Mansfeld, S. Lin, S. Kim, J. Shih:* J. Electrochem. Soc. *137* (1990) 78.
[12] *P. L. Cabot, J. A. Garrido, E. Pérez, A. H. Moreira, P. T. A. Sumodjo, W. Proud:* Electrochim. Acta *40* (1995) 447.
[13] *J. B. Bessone, D. R. Salinas, C. E. Mayer, M. Eber, W. J. Lorenz:* Electrochim. Acta *37* (1992) 2283.
[14] *W. J. Lee, S. I. Pyun, J. W. Yeon, K. S. Chun, I. K. Choi:* Mater. Sci. Forum *289–292* (1998) 915.
[15] *D. H. van der Weijde, E. P. M. van Westing, J. H. W. de Wit:* Corros. Sci. *36* (1994) 643.
[16] *J. H. W. de Wit, H. J. W. Lenderink, D. H. van der Weijde, E. P. M. van Westing:* Mater. Sci. Forum *192–194* (1995) 253.
[17] *P. L. Bonora, F. Deflorian, L. Fedrizzi:* Mater. Sci. Forum *192–194* (1995) 267.
[18] *D. H. van der Weijde, E. P. M. van Westing, J. H. W. de Wit:* Mater. Sci. Forum *289–292* (1998) 237.
[19] *C. C. Lee, F. Mansfeld:* Corr. Sci. *41* (1999) 439.
[20] *M. W. Kendig, H. S. Ryang, T. L. Liao, S. L. Jeanjaquet:* Corrosion *55* (1999) 222.
[21] *A. Conde:* PhD Thesis, Univ. Complutense, Madrid (Spain), 1996.
[22] *A. Conde, J. J. de Damborenea:* Corr. Sci. *39* (1997) 295.
[23] *M. Bethencourt, F. J. Botana, J. J. Calvino, G. Cifredo, M. Marcos, J. Pérez, M. A. Rodríguez:* Proc. V Reunión Nacional de Materiales, Paper B02029, p. 222, Cádiz (Spain), (1996).
[24] *M. Bethencourt, F. J. Botana, J. J. Calvino, M. Marcos, J. Pérez, M. A. Rodríguez-Chacón:* Electron Microscopy, Proc 14th ICEM 2 (1998) 103.
[25] *A. Aballe, M. Bethencourt, F. J. Botana, M. Marcos, J. Pérez, M. A. Rodríguez:* Rev. Metal. Madrid 34(mayo) (1998) 47.
[26] *A. Aballe, M. Bethencourt, F. J. Botana, J. Cano, M. Marcos:* Corr. Reviews *13* (2000) 1.
[27] *M. Bethencourt, F. J. Botana, J. J. Calvino, M. Marcos, J. Pérez, M. A. Rodríguez:* Mater. Sci. Forum *289–292* (1998) 567.
[28] *M. Bethencourt:* PhD. Thesis, Univ. Cádiz, Cádiz (Spain), 1999.
[29] *G. A. Ghering, M. H. Peterson:* Corrosion *37* (1981) 32.
[30] *J. O. Park, C. H. Paik, R. C. Alkire:* In: Critical Factors in Localized Corrosion II (Eds. P. M. Natishan, R. G. Kelly, G. S. Frankel, R. C. Newman), The Electrochem. Soc., Pennington, NJ (USA) 1996, 218.
[31] *K. Nisancioglu, K. J. Davanger, O. Strandmyr:* J. Electrochem. Soc. *137* (1990) 69.
[32] *J. R. Galvele, S. M. de Micheli, I. L. Muller, S. B. de Wexler, I. L. Alanis:* In: Critical Potentials for Localized Corrosion of Aluminium Alloys, NACE-3 (Eds. R. Staehle, B. Brown, J. Kruger, A. Agrawal) National Association of Corrosion Engineers, Houston (USA) 1974, 580.
[33] *S. M. Moon, S. I. Pyun:* Corr. Sci. *54* (1998) 546.
[34] *U. R. Evans:* In: The Corrosion and Oxidation of Metals (Ed. E. Arnold), London (UK), 1960.
[35] *J. M. Abd El Kader, A. M. Shams El Din:* Brit. Corros. J. *14* (1979) 41.
[36] *A. Barbucci, G. Cerisola, P. L. Cabot, P. L., G. Bruzzone:* Mater. Sci. Forum *289–292* (1998) 529.
[37] *D. H. van der Weijde, E. P. M. Van Westing, J. H. W. de Wit:* Corr. Sci. *36* (1994) 643.
[38] *E. P. M. van Westing, G. M. Ferrari, J. H. W. de Wit:* Electrochim. Acta *39* (1994) 899.
[39] *C. M. Abreu, M. Izquierdo, M. Keddam, X. R. Nóvoa, H. Takenouti:* Electrochim. Acta *41* (1996) 2405.
[40] *N. Xu, G. E. Thompson, J. L. Dawson, G. C. Wood:* Corr. Sci. *34* (1993) 479.

(Received: May 21, 2000) W 3479